Geophysical Prospecting, 2004, **52**, 183–195

Effective elastic properties of randomly fractured soils: 3D numerical experiments

Erik H. Saenger,* Oliver S. Krüger and Serge A. Shapiro

Freie Universität Berlin, Fachbereich Geophysik, Malteserstr. 74–100, Haus D, 12249 Berlin, Germany

Received September 2002, revision accepted January 2004

ABSTRACT

This paper is concerned with numerical tests of several rock physical relationships. The focus is on effective velocities and scattering attenuation in 3D fractured media. We apply the so-called rotated staggered finite-difference grid (RSG) technique for numerical experiments. Using this modified grid, it is possible to simulate the propagation of elastic waves in a 3D medium containing cracks, pores or free surfaces without applying explicit boundary conditions and without averaging the elastic moduli. We simulate the propagation of plane waves through a set of randomly cracked 3D media. In these numerical experiments we vary the number and the distribution of cracks. The synthetic results are compared with several (most popular) theories predicting the effective elastic properties of fractured materials. We find that, for randomly distributed and randomly orientated non-intersecting thin penny-shaped dry cracks, the numerical simulations of P- and S-wave velocities are in good agreement with the predictions of the self-consistent approximation. We observe similar results for fluid-filled cracks. The standard Gassmann equation cannot be applied to our 3D fractured media, although we have very low porosity in our models. This is explained by the absence of a connected porosity. There is only a slight difference in effective velocities between the cases of intersecting and non-intersecting cracks. This can be clearly demonstrated up to a crack density that is close to the connectivity percolation threshold. For crack densities beyond this threshold, we observe that the differential effective-medium (DEM) theory gives the best fit with numerical results for intersecting cracks. Additionally, it is shown that the scattering attenuation coefficient (of the mean field) predicted by the classical Hudson approach is in excellent agreement with our numerical results.

INTRODUCTION

The derivation and validation of accurate relationships between pore structure and elastic properties of porous rocks is an ongoing problem in geophysics, material science and solid mechanics. Understanding the interactions between rock, pore space and fluids, and how they control rock properties is crucial to a better understanding of acoustic and seismic data.

A range of different effective-medium theories (see Mavko, Mukerji and Dvorkin 1998 and references therein) give expressions for the overall properties of fractured media if the wavelength is large compared with the size of inclusions. There is a general agreement among these theories for a dilute concentration of inclusions. However, there are considerable differences for higher concentrations. Therefore, it is necessary to validate the different analytical predictions with experimental (e.g. Carvalho and Labuz 1996; Hudson, Pointer and Liu 2001) or numerical data.

With this in mind, Saenger and Shapiro (2002) presented efficient and accurate finite-difference (FD) computer simulations of wave propagation and effective elastic properties in 2D fractured media. The present

*E-mail: saenger@geophysik.fu-berlin.de

paper is an extension of this work to 3D fractured media.

Spring network techniques (e.g. Garboczi and Day 1995; Garboczi and Berryman 2001; Ursenbach 2001) provide an alternative numerical method for studying the elastic moduli of porous media. All these methods are currently restricted to isotropic materials where Poisson's ratio cannot be chosen arbitrarily. Attenuation effects also cannot be described with these methods, because they treat the static case only.

Finite-difference methods discretize the wave equation on a grid. They replace spatial derivatives by FD operators using neighbouring points. This discretization can cause instability problems on a staggered grid (Virieux 1986) when the medium contains high-contrast discontinuities (strong heterogeneities). These difficulties can be avoided by using the rotated staggered grid (RSG) technique (Saenger, Gold and Shapiro 2000). Since the FD approach is based on the wave equation without physical approximations, the method accounts not only for direct waves, primary reflected waves and multiply reflected waves, but also for surface waves, head waves, converted reflected waves, and diffracted waves observed in ray-theoretical shadow zones (Kelly *et al.* 1976). Additionally, it accounts for the proper relative amplitudes. Consequently, we use this numerical method for our considerations of 3D fractured materials.

This paper consists of two main parts. In the first part, we review several theoretical predictions of effective elastic properties of fractured media. In the second part, we validate the predictions numerically. We explain our simulation set-up with a detailed estimation of sources of errors, and discuss the numerical results.

THEORY

We consider wave propagation through a well-defined fractured region with thin penny-shaped cracks of equal form and size. For penny-shaped cracks (ellipsoids with two major axes of equal size), a distinction must be made between cracks with non-zero aspect ratio α and an aspect ratio equal to zero. The latter are referred to as disks. The commonly used crack-density parameter ρ used to characterize fractured materials is (Bristow 1960; Kachanov 1992)

$$\rho = \frac{1}{V_0} N a^3, \tag{1}$$

where N is the total number of cracks, V_0 is the representative volume element and a is the radius of the penny-shaped cracks. The porosity is

$$\phi = \frac{4}{3}\pi \frac{N}{V_0} a^2 d, \tag{2}$$

where a and d are the major axis (radius) and minor axis of the ellipsoid, respectively. If all cracks have the same ellipsoidal shape, the relationship between porosity ϕ and crack density ρ is (Cheng 1993)

$$\phi = \frac{4}{3}\pi\alpha\rho, \tag{3}$$

where $\alpha = d/a$ is the aspect ratio of penny-shaped ellipsoidal cracks.

Effective moduli of 3D fractured media with non-intersecting thin penny-shaped dry cracks

In order to describe wave propagation in fractured media, we consider four different theories for thin dry penny-shaped cracks in 3D media, namely, the Kuster–Toksöz formulation, the self-consistent approximation, the differential effective-medium (DEM) theory and the theory for non-interacting cracks. They can be used to predict effective wave velocities in the long-wavelength approximation as a function of porosity ϕ or crack density ρ. A detailed review of these rock physical relationships can be found in Mavko *et al.* (1998) and Kachanov (1992). Our aim is to investigate their limit of applicability for relatively high crack densities. Therefore, in order to compare our numerical results with these four theories, we give their respective effective bulk moduli $K^*(\phi)$ or effective Young's moduli $E^*(\phi)$ and effective shear moduli $\mu^*(\phi)$ in the Appendix.

Intersecting cracks

In the effective-medium theories mentioned above, the fractures are modelled as ellipsoidal cavities. As mentioned by Schoenberg and Sayers (1995), real fractures do not resemble isolated voids in a solid matrix. Borehole pictures, examination of outcrops, and rock fractured in the laboratory all indicate that fractures have many points of contact along their length. Therefore, we extend our numerical considerations to intersecting cracks. This is beyond the validity of most effective-medium theories.

For a random array of overlapping cracks, it is possible to define a connectivity percolation threshold ρ_{p}. At this crack density, the crack network allows fluid flow through the fractured rock. In the literature, we found three approaches with substantially different predictions of this value for thin penny-shaped cracks (disks), i.e.

$$\rho_p = 1.8/\pi^2 = 0.18 \quad \text{(Charlaix 1986)}, \tag{4}$$

$$\rho_p = 1.85/8 = 0.23 \quad \text{(Adler and Thovert 1999)}, \tag{5}$$

$$\rho_p = 3.0/\pi^2 = 0.30 \quad \text{(Garboczi \textit{et al.} 1995)}. \tag{6}$$

A discussion of the discrepancy between the three approaches can be found in Adler and Thovert (1999).

It is important to distinguish between the connectivity percolation threshold described above and the critical porosity (e.g. Nur 1992; Mukerji *et al.* 1995; Saenger and Shapiro 2002) at which rocks lose rigidity and fall apart. To our knowledge the determination of the critical porosity (or critical crack density ρ_r) for randomly orientated and randomly distributed thin penny-shaped cracks has not been documented in the literature. However, it is clear that the rigidity threshold characterized by ρ_r is much larger than the connectivity threshold ($\rho_r \gg \rho_p$).

Fluid-filled cracks

The Kuster–Tuksöz formulation, the self-consistent approximation and the DEM theory can be used also for fluid-filled cracks. For the exact analytical expressions we refer to the references given in the Appendix. Note that since the cavities are isolated with respect to flow, these approaches simulate the high-frequency behaviour of saturated rocks (the high-frequency limit of the squirt model). This should not be confused with the fact that these theories are often termed low-frequency theories as inclusion dimensions are assumed to be much smaller than a wavelength (Mavko *et al.* 1998).

If all cracks were connected, an alternative method for predicting effective moduli of fluid-filled fractured media would be the application of the Gassmann equation (Gassmann 1951). This connectivity is not given for the isolated penny-shaped cracks used in our models. However, we want to clarify numerically whether the Gassmann equation can be used for such cracks in the low-porosity limit.

NUMERICAL EXPERIMENTS

The propagation of elastic waves is described by the elastodynamic wave equation (e.g. Aki and Richards 1980):

$$\rho_g(\mathbf{r})\ddot{u}_i(\mathbf{r}) = (c_{ijkl}(\mathbf{r})u_{k,l}(\mathbf{r}))_{,j} + f_i(\mathbf{r}). \tag{7}$$

For modelling elastic waves at the position $\mathbf{r}$ using finite-differences, it is necessary to discretize the stiffness tensor c_{ijkl}, the (gravitational) density ρ_g, the displacement wavefield u_i and the body force f_i on a grid.

Numerical set-up

In order to test the different effective-medium theories mentioned above, we apply the so-called rotated staggered FD scheme to model wave propagation in fractured media (Saenger *et al.* 2000). Before comparing analytical predictions with numerical data, it is necessary to clarify the accuracy of the numerical calculations. After a detailed description of our modelling procedure, we then consider possible sources of numerical errors.

We design a number of numerical elastic models (details can be found in Table 1) that include a region with a known number of cracks and porosity. This fractured region (always from a depth of 173 gridpoints in the model) was filled at random with randomly orientated thin penny-shaped cracks. The implementation of the cracks on the 3D cubic FD grid is carried out by assigning crack properties to single neighbouring gridpoints. The best possible representation of a 3D thin penny-shaped crack gives a rough disk-like inclusion (due to discretization) with a thickness of one gridpoint. For models with non-intersecting cracks the same procedure as given by Davis and Knopoff (1995) and Dahm and Becker (1998) is used: if two cracks intersected during random selection, the more recent crack was eliminated and a random choice was made again. Figure 1 shows a typical model. All models are always discretized with an interval of 0.0002 m. In the homogeneous regions, we set $v_p = 5100$ m/s, $v_s = 2944$ m/s and $\rho_g = 2540$ kg/m^3. For the dry penny-shaped cracks, we set $v_p = 0$ m/s, $v_s = 0$ m/s and $\rho_g = 0.0001$ kg/m^3, which approximates a vacuum. For the case of fluid-filled penny-shaped cracks, we set $v_p = 1485$ m/s, $v_s = 0$ m/s and $\rho_g = 1000$ kg/m^3, which approximates water. It is important to note that we perform our modelling experiments with periodic boundary conditions in the two horizontal directions. For this reason our elastic models are also generated with this periodicity. Hence, it is possible for a single crack to start at the right side of the model and to end at its left side.

To obtain effective velocities in different models (with a different number of cracks), we apply a body force plane source at the top of the model. The plane wave generated in this way propagates through the fractured medium (see Fig. 2). With two horizontal planes of receivers at the top and at the bottom, it is possible to measure the time delay of the peak amplitude of the mean plane wave caused by the inhomogeneous region (i.e. the cracks). With this time delay, the effective velocity

Table 1 Crack models for numerical calculations. The models with an x attached to their number have intersecting cracks. Note that 0.0002 m is the size of grid spacing and N denotes the number of model realizations. The cracks can be fluid-filled or empty

Model no. (allocation number)	Number of cracks	Crack radius a [0.0002 m]	Size of cracked region [$(0.0002\ m)^3$]	Total height of model [0.0002 m]	Porosity ϕ of the crack region	Crack density ρ	N
1	20	31.5	400^3	805	0.0011	0.0098	1
2.1–2.3	40	31.5	400^3	805	0.0023	0.0195	3
3.1–3.3	80	31.5	400^3	805	0.0045	0.039	3
4.1–4.3	160	31.5	400^3	805	0.0090	0.078	3
5	240	31.5	400^3	805	0.0135	0.117	1
6.1–6.3	320	31.5	400^3	805	0.0180	0.156	3
7.1–7.3	60	31.5	$300^2 \times 400$	1305	0.0060	0.052	3
8.1–8.3	30	41.5	$250^2 \times 500$	1305	0.0060	0.069	3
9.1x–9.3x	80	31.5	400^3	805	0.0044	0.039	3
10.1x–10.3x	160	31.5	400^3	805	0.0089	0.078	3
11.1x – 11.5x	320	31.5	400^3	805	0.0179	0.156	5
12.1x–12.2x	700	31.5	400^3	805	0.038	0.342	1
13x	1000	31.5	400^3	805	0.054	0.488	1
14.1x–14.2x	1200	31.5	400^3	805	0.065	0.585	2
15.1x–15.2x	2000	31.5	400^3	805	0.106	0.977	2

can be estimated (see Fig. 3). Additionally, the attenuation of the plane wave can be studied. The source wavelet in our experiments is always the first derivative of a Gaussian with a dominant frequency of 8×10^5 Hz and a time increment of $\Delta t = 2.1 \times 10^{-8}$ s. The resulting power spectrum of the plane P-wave is shown in Fig. 4. Due to the size of the models we have to use large-scale computers (e.g. CRAY T3E) with an MPI implementation of our modelling software. In fact, the size restriction on our models is mainly due to computational restrictions in memory and CPU time.

Similarly to Garboczi and Berryman (2001), Ursenbach (2001) and Arns (2002), we detect three main sources of error in our numerical calculations: (1) the finite-size effect, (2) digital resolution and (3) statistical variation. Two other sources of error, specific for finite-difference solutions of the elastodynamic wave equation, are (4) numerical dispersion and (5) the general modelling accuracy for high-contrast inclusions.

1 Finite-size errors result from having a sample (fractured region) of finite size, where the largest length scales of inclusions are of the order of the sample size. Samples at this scale can no longer be representative and the numerical data become noisy. Experience with many previous results (Garboczi and Berryman 2001; Saenger and Shapiro 2002) has shown that when the ratio of the sample size to the diameter of the penny-shaped crack is about 7, finite-size errors are negligible.

2 The digital-resolution error is caused by using a rectangular finite-difference grid. The crack geometries have to be represented on this given grid structure. We observe only very small variations among the different crack sizes we have used (shown below). An important argument in favour of the digital-resolution error being below an acceptable level is the fact that for low crack densities all theories and numerical results are in a good agreement. However, this error is the most critical error in our numerical measurements (and in the similar studies of Garboczi and Berryman (2001), Ursenbach (2001) and Arns (2002)).

3 The statistical-variation error occurs because the models under consideration are random. For a given crack density, there are many ways in which the cracks might be randomly arranged. In general, each arrangement will have somewhat different effective elastic moduli. The error bar in our numerical results denotes the standard deviation for different model realizations. It can be observed that this deviation is always very small.

4 In order to reduce the dispersion error of the FD simulations, we use only 54% of the allowed maximum time increment ($\gamma = 0.54\gamma_{\max}$; see Saenger *et al.* 2000). All computations are performed with second-order spatial FD operators and with a second-order time update. The number of gridpoints per wavelength N_λ is equal to or greater than 100. Therefore, with this configuration, our

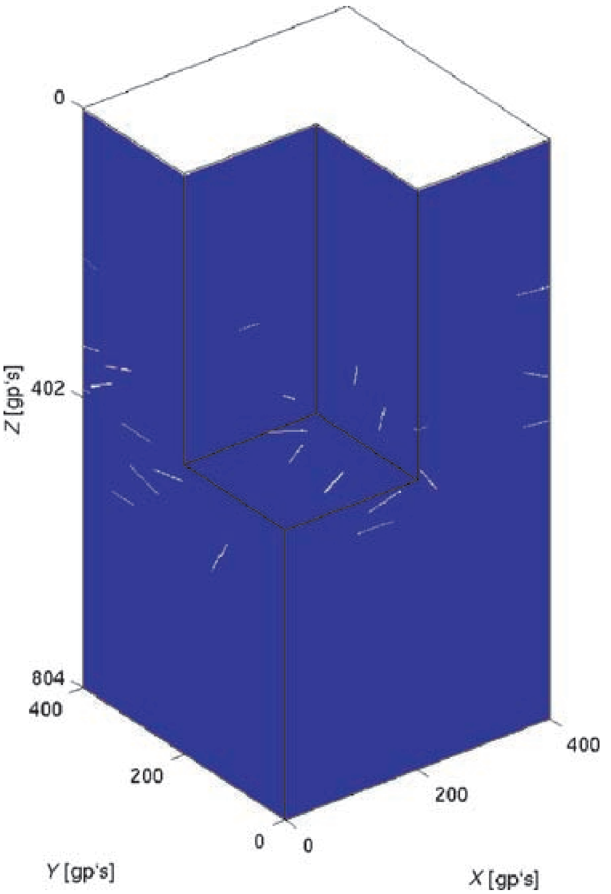

Figure 1 A typical 3D fractured model with non-intersecting penny-shaped cracks (radius $r = 31.5$ gridpoints) used for the numerical experiments. We introduce a cracked region ($400 \times 400 \times 400$ gridpoints) into a homogeneous material. At the top we place a small strip of vacuum. This is advantageous for applying a body force plane source with the rotated staggered grid.

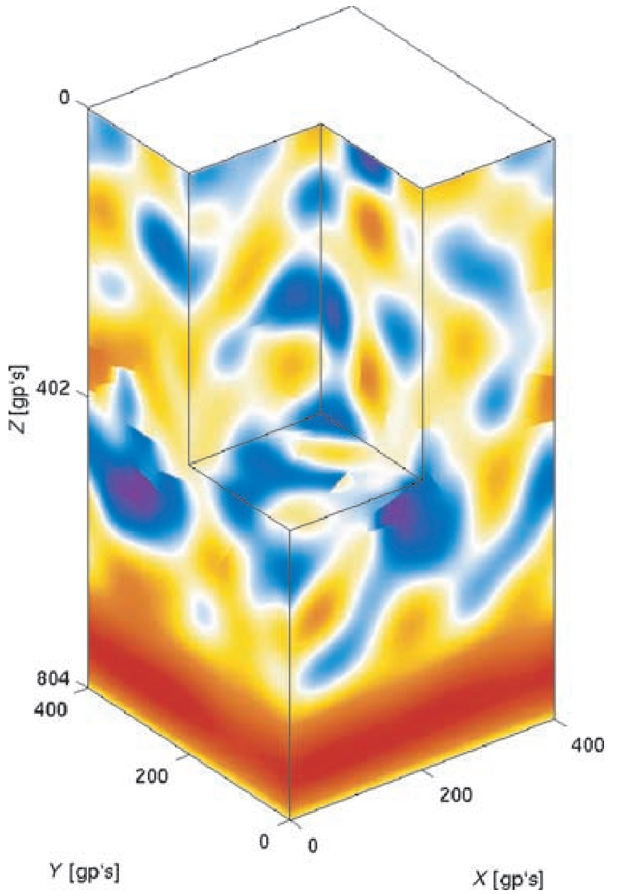

Figure 2 A z-displacement snapshot of a plane P-wave propagating through the fractured 3D model. We use a non-linear colour scale to emphasize the scattered wavefield. The visible discontinuities of the wavefield correspond to the crack locations (compare with Fig. 1).

measurements are for a homogeneous model with crack density $\rho = 0$, velocity $v_p = 5102.91$ m/s (error relative to the input velocity of 5100 m/s: 0.057%) and $v_s = 2943.62$ m/s (error relative to the input velocity of 2944 m/s: 0.004%).

5 Krüger, Saenger and Shapiro (2002) studied the numerical accuracy of the rotated staggered grid (RSG) for high-contrast inclusions. They compared the analytically and numerically derived power spectra and seismograms of SH-wave diffraction by a finite plane crack. Both approaches, the analytical solution of Sánchez-Sesma and Iturrarán-Viveros (2001) and the numerical solution using the RSG, show an excellent correspondence. A remarkable aspect is that for inclined cracks the numerical solution is still correct, even though the crack is discretized on a grid and does not have a perfect plane surface.

Scattering attenuation for non-intersecting dry penny-shaped cracks

In this section we consider the scattering attenuation coefficient (equation (A1)) predicted by Hudson (1981). In contrast to the velocity considerations, we are interested to record the complete transmitted plane wave. From the numerical point of view, it is necessary to modify the standard model size (used for velocity considerations). Therefore we use the models 7.1–7.3 with an extended total height (Table 1).

The frequency-dependent relative attenuation A is calculated by dividing the Fourier transform of the transmitted mean field of the plane wave (solid trace in Fig. 3) by the

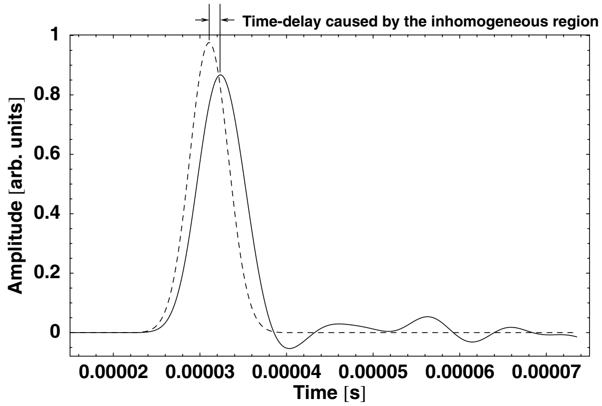

Figure 3 The mean field (average of 400^2 receivers) recorded at the bottom of the 3D model (compare with Figs 1 and 2). The dotted line is recorded in a homogeneous model without cracks. The solid line is recorded within a heterogeneous model, i.e. the fractured model 7.1 (Table 1). Using the time delay, the effective velocity in the fractured region can be estimated. The scattering attenuation due to the cracks can be calculated by analysing the ratio of the Fourier transform of both traces.

power spectrum of the incident plane wave (dashed trace in Fig. 3). Additionally, the attenuation coefficient γ is estimated by using $\gamma = -(\ln A)/L$ (L denotes the length of the travelpath). A comparison of the results of the Hudson approach and our numerical results is shown in Fig. 4. We observe a good agreement. The systematic oscillations in the numerical results can be explained by the relatively short travelpath through the fractured media and by internal oscillations. Note that the observed typical Rayleigh scattering is an additional indication that our simulations represent the long-wavelength limit. This is important because all effective-medium theories considered below are valid only in the long-wavelength limit.

Numerical results for effective P- and S-wave velocities for non-intersecting dry penny-shaped cracks

Our numerical results for penny-shaped dry cracks are depicted by dots in Figs 5 and 6. We show the relative decrease in the normalized effective P- and S-wave velocities as a function of the crack density ρ. For the case of non-intersecting cracks we use models nos 1, 2.1–2.3, 3.1–3.3, 4.1–4.3, 6.1–6.3, 7.1–7.3, 8.1–8.3 for P-waves and models nos 3.1, 4.1, 5, 6.1, 6.2 for S-waves (Table 1). For comparison, the predictions of the four theories described in the Appendix are also shown. Note that it is not useful to study crack densities higher than the connectivity percolation threshold (equations (4), (5) and (6)) for non-intersecting cracks. For those high crack densities, it is problematic to generate high-order statistically independent crack models (too many cracks must be removed in the model build-up process).

The first conclusion is that none of the theories provide precise results for relatively high crack densities. Overall, they tend to underestimate the effect of velocity reduction by empty cracks. This can be particularly clearly observed in the theory of non-interacting cracks by Kachanov (1992). The best match to the numerical estimates is given by the self-consistent approximation (O'Connell and Budiansky 1974). This is most significant for the effective P-wave velocities. A comparison with experimental data described in a recent review of Hudson's model for cracked media (Hudson *et al.* 2001) provides a similar conclusion. As mentioned in the Appendix, the self-consistent approximation for randomly orientated inclusions agrees with the first-order corrections predicted by Hudson (1981).

At a first glance, our 3D results seem to be in conflict with the numerical results of 2D fractured media presented by Saenger and Shapiro (2002). In contrast to the 3D results, they support the *modified self-consistent theory* (similar to DEM) for relative high crack densities. However, a closer look at the 2D results (Fig. 2 of Saenger and Shapiro 2002) shows that, at slightly higher crack densities (in a middle range), the self-consistent theory and the numerical results are also in good agreement. A general underestimation of velocity reduction by empty cracks using the 2D theory for non-interacting cracks by Kachanov (1992) can also be observed. Therefore, we assert that the 2D and 3D results complement each other.

Numerical results for effective P-wave velocities for intersecting dry penny-shaped cracks

For intersecting cracks, it is not difficult to generate statistically independent models with high crack densities because it is not necessary to eliminate intersecting cracks in the random generation process. The details of the models used, nos 9.1x–9.3x, 10.1x–10.3x, 11.1x–11.5x, 12.1x, 12.2x, 13x, 14.1x, 14.2x, 15.1x, 15.2x with intersecting cracks, can be found in Table 1. The 3D numerical results for the normalized effective P-wave velocities for thin penny-shaped dry cracks are shown in Fig. 7.

It is interesting to observe that the connectivity percolation threshold (equations (4), (5) and (6)) cannot be clearly detected in the seismic signatures of the numerical experiments. The difference between effective velocities for

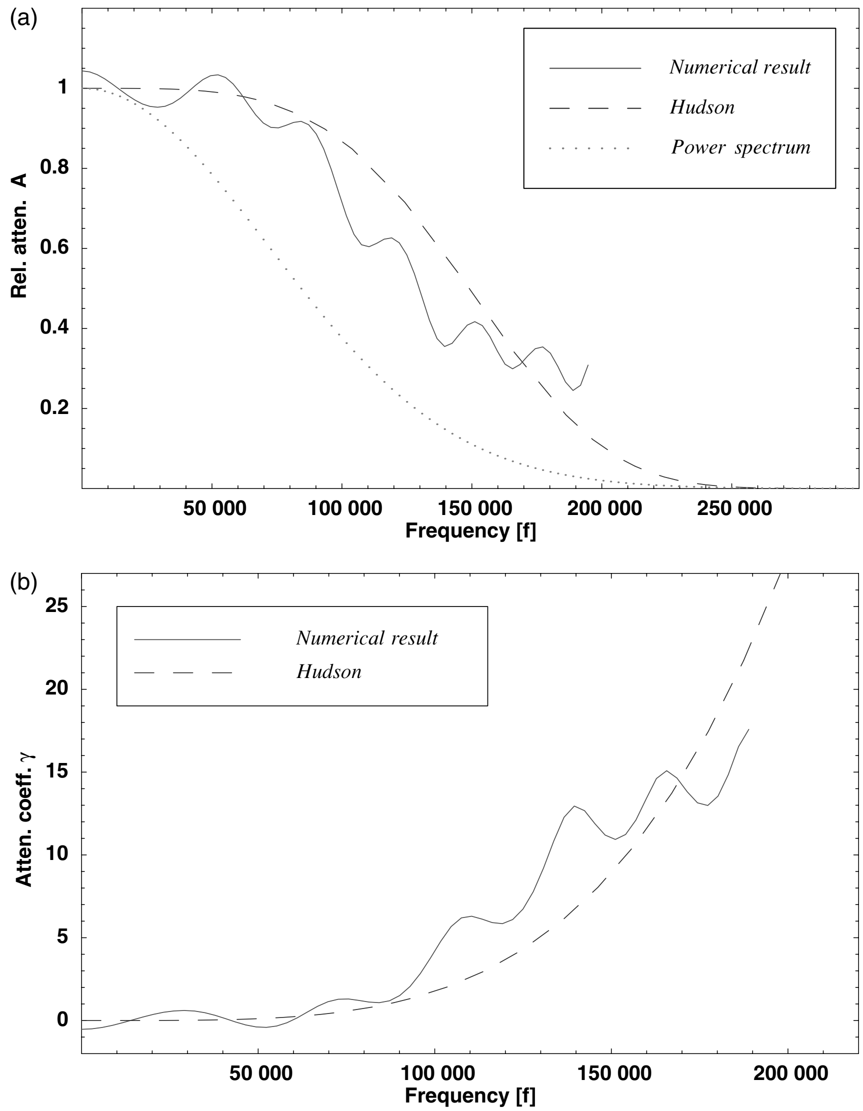

Figure 4 (a) The solid line depicts the ratio between power spectra of transmitted (through the region with empty penny-shaped cracks) and incident signals of the P-wave. The dashed line shows the same quantity predicted by Hudson (1981) using equation (A1). The dotted line is the normalized power spectrum of the generated plane P-wave of the simulation. The frequency corresponding to the wavelength equal to the diameter of the cracks is $f = v_{\mathrm{P}}/(2a) =$ 425 000 Hz. The crack density of the corresponding three models is $\rho = 0.045$. (b) As (a), but now the attenuation coefficient γ_{P} is depicted. The fourth-power dependence on the frequency f of Rayleigh scattering can be clearly observed.

intersecting or non-intersecting cracks is not significant for crack densities below this range. Although the effective-medium theories described above are not derived for intersecting cracks, we test their applicability for such media. Therefore, for comparison the predictions of these theories are also shown in Fig. 7. For the self-consistent approximation and the Kuster–Toksöz approach, a non-physical cut-off crack density ρ_{cf} can be estimated. At this crack density the theories predict an effective velocity of zero for P- and S-waves. This cut-off crack density is not related to the rigidity percolation threshold ρ_{r}.

Again, as for non-intersecting cracks, none of the theories provide precise results for high crack densities. However, the best fit between numerical results for high crack densities and the theoretical predictions is given by the DEM theory. Along with the assumption $\rho_{\mathrm{r}} \gg \rho_{\mathrm{p}}$ (see Section 'Intersecting cracks'), this is again consistent with the findings of Saenger and Shapiro (2002).

Numerical results for effective P- and S-wave velocities for non-intersecting fluid-filled penny-shaped cracks

For the calculations of the effects of penny-shaped fluid-filled cracks, we have used models nos 3.1–3.3, 4.1, 6.1–6.3 for P-waves and nos 3.1, 4.1, 5, 6.1, 6.2 for S-waves (Table 1). The relative decrease in the normalized effective P- and S-wave velocities as a function of the crack density ρ is shown in Figs 8 and 9. For comparison, the three effective-medium theories for

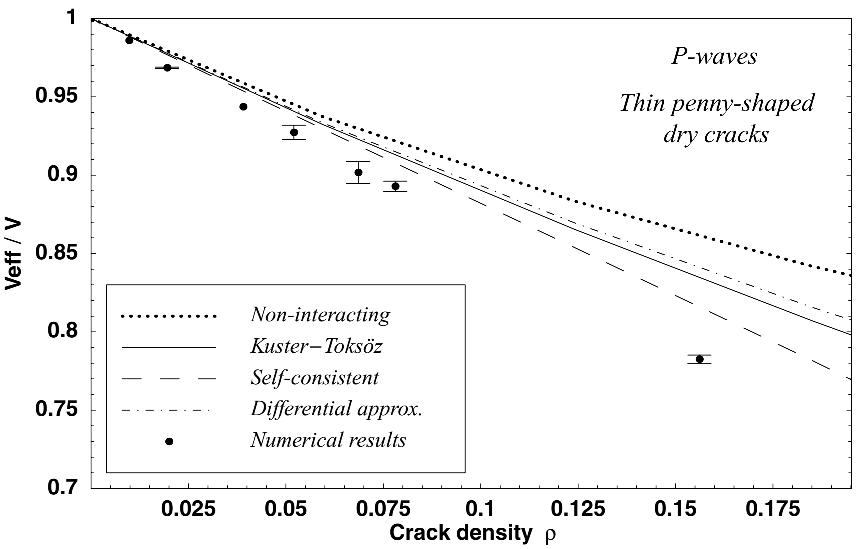

Figure 5 Normalized effective velocity of P-waves versus crack density ρ of penny-shaped cracks. Dots: numerical results of this study. The error bars denote the standard deviation for different model realizations (see Table 1). The dotted and the dashed-dotted lines are predicted by the theory of non-interacting cracks and the DEM theory, respectively. The solid line is the prediction by the Kuster–Toksöz approach and the dashed line is due to the self-consistent approximation.

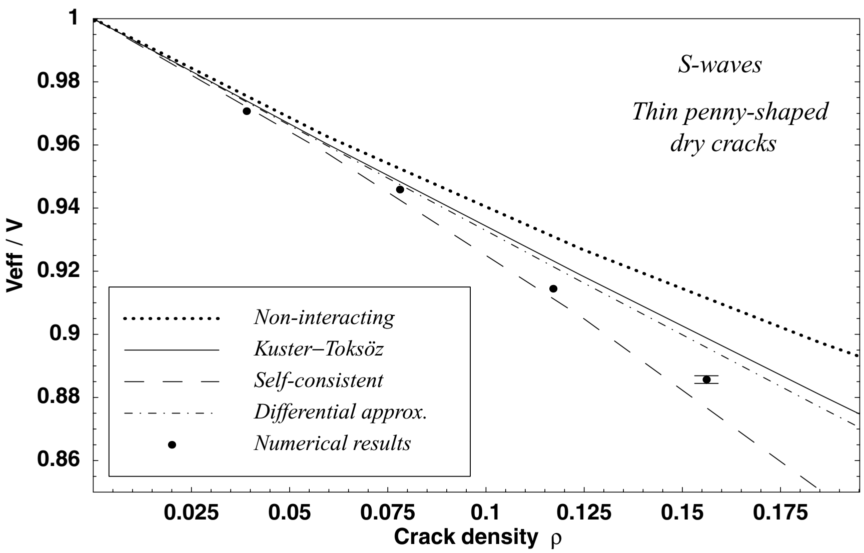

Figure 6 As Fig. 5 for S-waves.

isolated fluid-filled cracks discussed in the Section 'Fluid-filled cracks' are also displayed.

From the numerical point of view, it is not possible to distinguish unambiguously which effective-medium theory gives the best prediction. The differences between the theoretical approaches for the investigated crack densities are very small. Once again, as for empty cracks, the trend of the theories to underestimate the effect of velocity reduction caused by the inclusions can be detected. There is only a slight indication that the self-consistent approach is superior to the other theories.

Additionally, with our numerical considerations we can address the Gassmann equation. We restrict ourselves to studying fluid effects on wave propagation in the case of non-intersecting cracks. Fluid flow is not possible between them. Therefore, we do not fulfil one basic assumption of the Gassmann equation (compare with Wang 2000). However, in this study we want to give a quantitative illustration of how far Gassmann's predictions can deviate from the effective moduli of a medium with isolated fluid inclusions.

First, we compare a combination of the self-consistent theory estimate of the dry rock moduli with the Gassmann formalism to numerically derived P- and S-wave velocities. The expected disagreement between this theoretical prediction and our numerical results can clearly be detected in Figs 8 and 9.

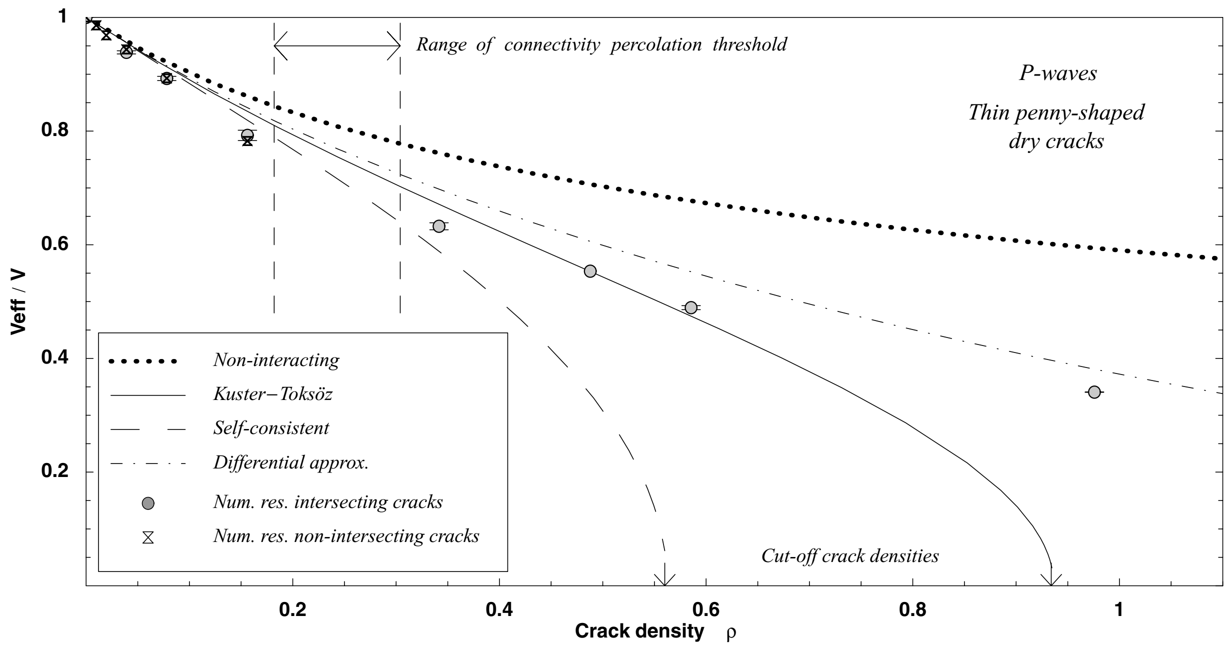

Figure 7 Normalized effective velocity of P-waves versus crack density ρ for intersecting and non-intersecting penny-shaped cracks. Dots: numerical results for intersecting cracks. The error bars (here only shown for the case of intersecting cracks) denote the standard deviation for different model realizations (see Table 1). Double triangles: numerical results for non-intersecting cracks. The dotted and the dashed-dotted lines are predicted by the theory of non-interacting cracks and the DEM theory, respectively. The solid line is the prediction by the Kuster–Toksöz approach and the dashed line represents the self-consistent approximation. The cut-off crack densities of the self-consistent approximation and the Kuster–Toksöz approach are $\rho_{\mathrm{cf}} = 0.56$ and $\rho_{\mathrm{cf}} = 0.93$, respectively. The vertical dashed lines display the range of the connectivity percolation threshold (see Section 'Intersecting cracks').

Figure 8 Normalized effective velocity of P-waves versus crack density ρ of fluid-filled non-intersecting penny-shaped cracks. Dots: numerical results of this study. The error bars denote the standard deviation for different model realizations (see Table 1). The dashed-dotted line is predicted by the DEM theory. The solid line is the prediction using the Kuster–Toksöz approach and the dashed line is due to the self-consistent approximation. The dotted line is found by taking the self-consistent effective moduli for dry cracks and saturating them with the Gassmann equation.

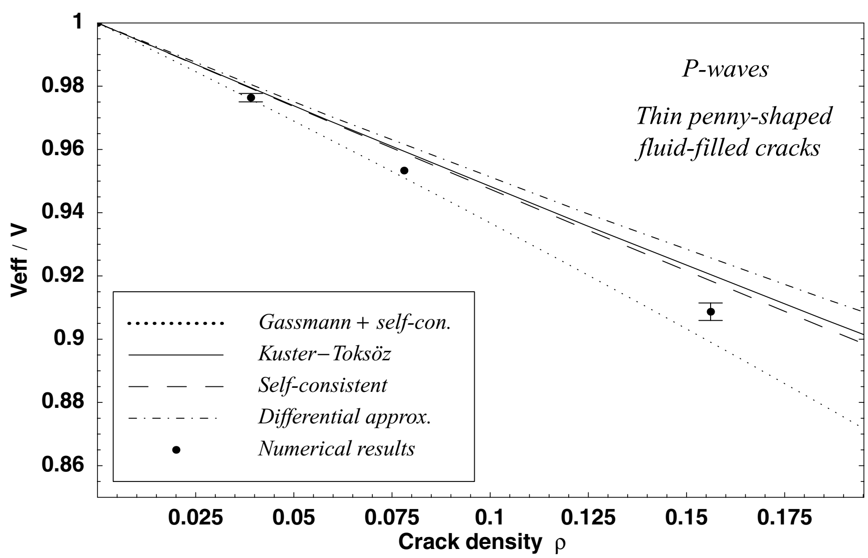

On the other hand, our numerical set-up enables us to study 3D fractured media using exactly the same crack positions for both fluid-filled and empty cracks (i.e. the dry rock frame is exactly the same in both simulations). Therefore, we can test the applicability of the Gassmann equation for our 3D fractured materials without any additional effective-medium theory. The calculated normalized effective shear moduli μ^* for fluid-filled and for empty non-intersecting

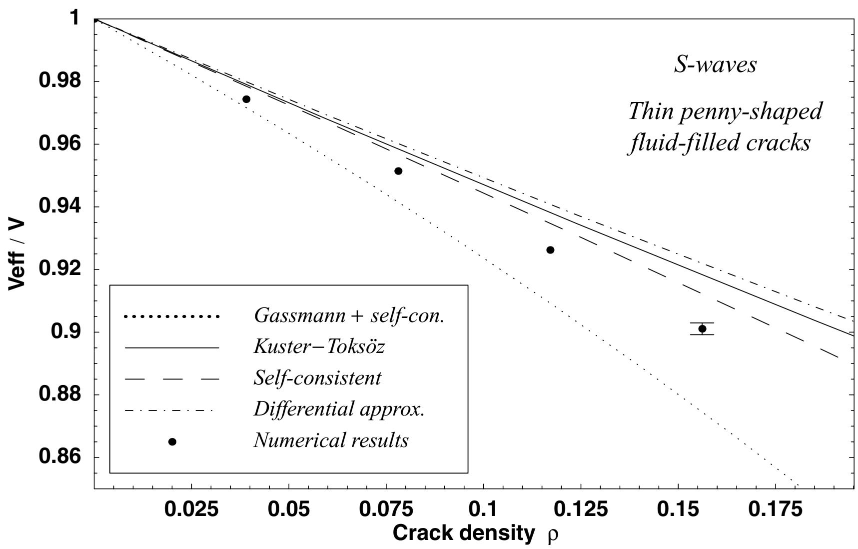

Figure 9 As Fig. 8 for S-waves.

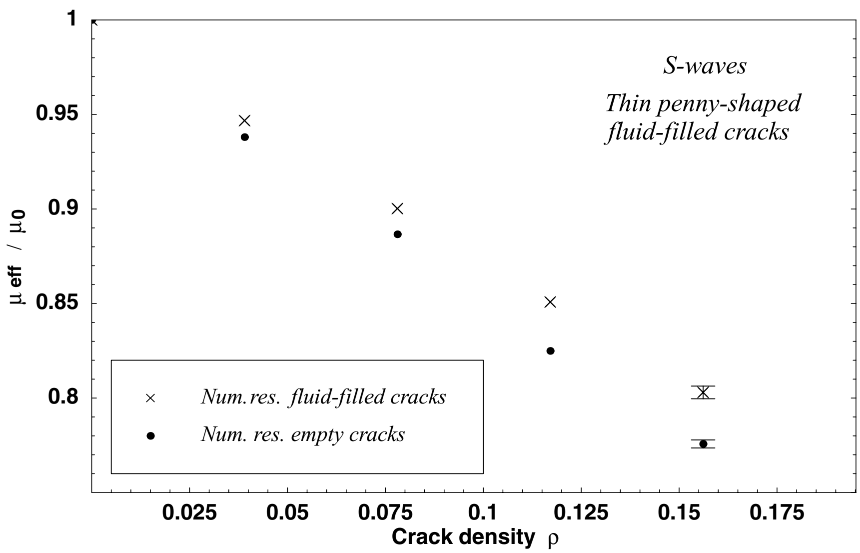

Figure 10 Normalized effective shear moduli μ^* calculated from the effective shear-wave velocities depicted in Figs 6 and 9. The dry rock frame is exactly the same for the models used with empty (depicted with dots) and fluid-filled (depicted with crosses) cracks.

cracks are compared in Fig. 10. There is a significant difference between both moduli. The equality predicted by (A19) cannot be observed. Note that this result is obtained for crack densities below the range of the connectivity percolation threshold for intersecting cracks. This brings us to the conclusion that the Gassmann equation cannot be applied to isolated fluid-filled cracks, even with low porosity in the models used.

CONCLUSIONS

Finite-difference modelling of the elastodynamic wave equation is very fast and accurate. We used the rotated staggered FD grid to calculate elastic wave propagation in fractured media. Our numerical modelling of elastic properties of dry and fluid-saturated rock skeletons can be considered as an efficient and well-controlled computer experiment. We considered 3D isotropic fractured media with ellipsoidal inclusions.

We have numerically tested the effective-velocity predictions of different theoretical approaches. These were the theory for non-interacting cracks, the Kuster–Toksöz approach, the self-consistent theory, the differential effective-medium (DEM) theory and the Gassmann equation. For non-intersecting dry and fluid-filled penny-shaped cracks at slightly higher crack densities (below the connectivity percolation threshold for intersecting cracks), the self-consistent theory is most successful in predicting effective velocities for P- and S-waves. The

Gassmann equation cannot be applied to isolated fluid-filled cracks, even in the case of low porosity.

The more realistic assumption (with respect to natural rocks) of intersecting cracks is not included in the effective-medium theories described above. However, below the range of the connectivity percolation threshold, the difference in effective velocities for intersecting and non-intersecting cracks is negligible. For crack densities beyond this range, the DEM (not derived for intersecting cracks) is the best to apply.

Additionally, we have studied scattering attenuation of the mean field. The attenuation coefficient predicted by Hudson (1981) can be used for ellipsoidal high-contrast inclusions.

ACKNOWLEDGEMENTS

We thank the Deutsche Forschungsgemeinschaft (contract SH 55/2-2) and the Wave Inversion Technology (WIT) Consortium project for their financial support. We thank M. Karrenbach for providing us with his FD program for further modifications. The simulations were performed at the HLR Stuttgart (Project 12720).

REFERENCES

Adler P.M. and Thovert J.-F. 1999. *Fractures and Fracture Networks*. Kluwer Academic Publishers, Dordrecht.

Aki K. and Richards P.G. 1980. *Quantitative Seismology: Theory and Methods*. W.H. Freeman & Co.

Arns C.H. 2002. *The influence of morphology on physical properties of reservoir rocks*. PhD thesis, University of New South Wales.

Berryman J.G. 1992. Single-scattering approximations for coefficients in Biot's equations of poroelasticity. *Journal of the Acoustical Society of America* **91**, 551–571.

Bristow J. 1960. Microcracks and the static and dynamic elastic constants of annealed and heavily cold-worked metals. *British Journal of Applied Physics* **11**, 81–85.

Carvalho F.C.S. and Labuz F.J. 1996. Experiments on effective elastic modulus of two-dimensional solids with cracks and holes. *International Journal of Solids and Structures* **33**, 4119–4130.

Charlaix E. 1986. Percolation threshold of a random array of discs: a numerical simulation. *Journal of Physics A* **19**, L533–L536.

Cheng C.H. 1993. Crack models for a transversely isotropic medium. *Journal of Geophysical Research* **98**(B1), 675–684.

Dahm T. and Becker T. 1998. On the elastic and viscous properties of media containing strongly interacting in-plane cracks. *Pure and Applied Geophysics* **151**, 1–16.

Davis P.M. and Knopoff L. 1995. The elastic modulus of media containing strongly interacting antiplane cracks. *Journal of Geophysical Research* **100**, 18253–18258.

Douma J. 1988. The effect of the aspect ratio on crack-induced anisotropy. *Geophysical Prospecting* **36**, 614–632.

Garboczi E.J. and Berryman J.G. 2001. Elastic moduli of a material containing composite inclusions: Effective medium theory and finite element computations. *Mechanics of Materials* **33**, 455–470.

Garboczi E.J. and Day A.R. 1995. Algorithm for computing the effective linear elastic properties of heterogeneous materials: Three-dimensional results for composites with equal phase Poisson ratios. *Journal of Mechanics and Physics of Solids* **43**, 1349–1362.

Garboczi E.J., Snyder K.A., Douglas J.F. and Thorpe M.F. 1995. Geometrical percolation threshold of overlapping ellipsoids. *Physical Review E* **52**, 819–828.

Gassmann F. 1951. Über die Elastizität poröser Medien. *Vier. der Natur Gesellschaft* **96**, 1–23.

Grechka V. and Tsvankin I. 2003. Feasibility of seismic characterization of multiple fracture sets. *Geophysics* **68**, 1399–1407.

Hashin Z. and Shtrikman S. 1963. A variational approach to the elastic behavior of multiphase materials. *Journal of Mechanics and Physics of Solids* **11**, 127–140.

Hudson J.A. 1981. Wave speeds and attenuation of elastic waves in material containing cracks. *Geophysical Journal of the Royal Astronomical Society* **64**, 133–150.

Hudson J.A., Pointer T. and Liu E. 2001. Effective-medium theories for fluid-saturated materials with aligned cracks. *Geophysical Prospecting* **49**, 509–522.

Kachanov M. 1992. Effective elastic properties of cracked solids: critical review of some basic concepts. *Applied Mechanical Review* **45**, 304–335.

Kelly K.R., Ward R.W., Treitel S. and Alford R.M. 1976. Synthetic seismograms: a finite-difference approach. *Geophysics* **41**, 2–27.

Krüger O.S., Saenger E.H. and Shapiro S.A. 2002. Simulation of the diffraction by single cracks: an accuracy study. 72nd SEG meeting, Salt Lake City, USA, Expanded Abstracts, 2007–2010.

Kuster G.T. and Toksöz M.N. 1974. Velocity and attenuation of seismic waves in two-phase media: Part I: Theoretical formulations. *Geophysics* **39**, 587–606.

Mavko G., Mukerji T. and Dvorkin J. 1998. *The Rock Physics Handbook*. Cambridge University Press.

Mukerji T., Berryman J., Mavko G. and Berge P. 1995. Differential effective medium modeling of rock elastic moduli with critical porosity constraints. *Geophysical Research Letters* **22**, 555–558.

Norris A.N. 1985. A differential scheme for the effective moduli of composites. *Mechanics of Materials* **4**, 1–16.

Nur A. 1992. Critical porosity and the seismic velocities in rocks (abstract). *EOS Transactions AGU* **73**, 66.

O'Connell R.J. and Budiansky B. 1974. Seismic velocities in dry and saturated cracked solids. *Journal of Geophysical Research* **79**, 5412–5426.

Saenger E.H., Gold N. and Shapiro S.A. 2000. Modeling the propagation of elastic waves using a modified finite-difference grid. *Wave Motion* **31**, 77–92.

Saenger E.H. and Shapiro S.A. 2002. Effective velocities in fractured media: A numerical study using the rotated staggered finite-difference grid. *Geophysical Prospecting* **50**, 183–194.

Sánchez-Sesma F.J. and Iturrarán-Viveros U. 2001. Scattering and diffraction of SH waves by a finite crack: an analytical solution. *Geophysical Journal International* **145**, 749–758.

Schoenberg M. and Sayers C.M. 1995. Seismic anisotropy of fractured rock. *Geophysics* **60**, 204–211.

Ursenbach C.P. 2001. Simulation of elastic moduli of porous media. 71st SEG meeting, San Antonio, Texas, USA, Expanded Abstracts, 1704–1707.

Virieux J. 1986. Velocity-stress finite-difference method. *Geophysics* **51**, 889–901.

Wang Z. 2000. The Gassmann equation revisited: comparing laboratory data with Gassmann's predictions. In: *Seismic and Acoustic Velocities in Reservoir Rocks* (eds Z. Wang and A. Nur), pp. 8–23. Society of Exploration Geophysicists.

Zimmermann R.W. 1991. *Compressibility of Sandstones*. Elsevier Science Publishing Co.

APPENDIX

Scattering attenuation

Among other theoretical results, Hudson (1981) presented the attenuation coefficient ($\gamma_\mathrm{p} = \omega Q^{-1}/2v_\mathrm{p}$, where Q denotes quality factor) for the mean field of elastic waves in fractured media. For randomly orientated cracks (isotropic distribution), the P-wave attenuation coefficient is given as

$$\gamma_\mathrm{p} = \frac{\omega}{v_\mathrm{s}}\rho\left(\frac{\omega a}{v_\mathrm{p}}\right)^3 \frac{4}{225\pi}\left[AU_1^2 + \frac{1}{2}\frac{v_\mathrm{p}^5}{v_\mathrm{s}^5}B(B-2)U_3^2\right], \tag{A1}$$

where

$$A = \frac{3}{2} + \frac{v_\mathrm{s}^5}{v_\mathrm{p}^5}, \tag{A2}$$

$$B = 2 + \frac{15}{4}\frac{v_\mathrm{s}}{v_\mathrm{p}} - 10\frac{v_\mathrm{s}^3}{v_\mathrm{p}^3} + 8\frac{v_\mathrm{s}^5}{v_\mathrm{p}^5}, \tag{A3}$$

$$U_1 = \frac{16(\lambda+2\mu)}{3(3\lambda+4\mu)}, \tag{A4}$$

$$U_3 = \frac{4(\lambda+2\mu)}{3(\lambda+\mu)}. \tag{A5}$$

The isotropic background elastic moduli are λ and μ (Lamé parameters), while v_p and v_s denote the P- and S-wave velocities, respectively. The fourth-power dependence on angular frequency ω is characteristic of Rayleigh scattering, which can only be observed if the wavelength is large compared to the dimension of the scatterers.

Effective-medium theories

In order to compare our numerical results with the effective-medium theories mentioned in the Section 'Theory', we give here their respective effective bulk modulus $K^*(\phi)$ or effective Young's modulus $E^*(\phi)$ and effective shear modulus $\mu^*(\phi)$. For the case of penny-shaped dry cracks with aspect ratio α, the following formulae can be obtained, where K_m, E_m and μ_m are the bulk modulus, Young's modulus and the shear modulus, respectively, of the homogeneous background medium.

Kuster and Toksöz (1974) derived expressions for effective elastic properties using a long-wavelength first-order scattering theory. They are formally limited to low porosity and are as follows:

$$(K^*(\phi) - K_\mathrm{m})\frac{K_\mathrm{m} + \frac{4}{3}\mu_\mathrm{m}}{K^*(\phi) + \frac{4}{3}\mu_\mathrm{m}} = -\phi K_\mathrm{m} P_\mathrm{m}, \tag{A6}$$

$$(\mu^*(\phi) - \mu_\mathrm{m})\frac{\mu_\mathrm{m} + \zeta_\mathrm{m}}{\mu^*(\phi) + \zeta_\mathrm{m}} = -\phi\mu_\mathrm{m} Q_\mathrm{m}, \tag{A7}$$

where

$$P_\mathrm{m} = \frac{K_\mathrm{m}}{\pi\alpha\beta_\mathrm{m}}, \tag{A8}$$

$$Q_\mathrm{m} = \frac{1}{5} * \left[1 + \frac{8\mu_\mathrm{m}}{\pi\alpha(\mu_\mathrm{m} + 2\beta_\mathrm{m})} + \frac{4\mu_\mathrm{m}}{3\pi\alpha\beta_\mathrm{m}}\right], \tag{A9}$$

and

$$\beta = \mu\frac{3K+\mu}{3K+4\mu}, \tag{A10}$$

$$\zeta = \frac{\mu}{6}\frac{9K+8\mu}{K+2\mu}. \tag{A11}$$

In the self-consistent approximation (O'Connell and Budiansky 1974), the mathematical solution for the deformation of isolated inclusions is still used, but the interaction of inclusions is approximated by replacing the background medium with the *a priori* unknown effective medium (P and Q are given above), so that

$$K^*(\phi) = K_\mathrm{m}(1 - \phi P^*), \tag{A12}$$

$$\mu^*(\phi) = \mu_\mathrm{m}(1 - \phi Q^*). \tag{A13}$$

Note that the self-consistent approximation for randomly orientated inclusions agrees with the first-order corrections predicted by Hudson (1981).

The differential effective-medium (DEM) theory models two-phase composites by incrementally adding inclusions of one phase to the matrix phase (e.g. Zimmermann 1991). The predictions can be expressed by two coupled linear differential equations with initial conditions $K^*(0) = K_\mathrm{m}$ and $\mu^*(0) = \mu_\mathrm{m}$, which can be solved numerically (Berryman 1992):

$$(1-\phi)\frac{\mathrm{d}}{\mathrm{d}\phi}[K^*(\phi)] = -K^*(\phi)P^*, \tag{A14}$$

$$(1-\phi)\frac{\mathrm{d}}{\mathrm{d}\phi}[\mu^*(\phi)] = -\mu^*(\phi)Q^*. \tag{A15}$$

Norris (1985) showed that the DEM is realizable and therefore is always consistent with the Hashin–Shtrikman upper and lower bounds (Hashin and Shtrikman 1963).

The low aspect ratio of ellipsoidal cracks we used in our considerations makes it possible to compare the results with effective-medium theories constructed only for (flat) disks. The difference between low aspect ratio ellipsoidal inclusions and disks does not significantly influence the predictions of the three theories discussed above (compare with Douma 1988). Hence, we include in our comparison of theories the theory of non-interacting cracks (disks) of Kachanov (1992):

$$E^*(\rho) = E_\mathrm{m}\left[1 + \frac{16\left(1-\nu_\mathrm{m}^2\right)(1-3\nu_\mathrm{m}/10)}{9(1-\nu_\mathrm{m}/2)}\rho\right]^{-1}, \tag{A16}$$

$$\mu^*(\rho) = \mu_\mathrm{m}\left[1 + \frac{16(1-\nu_\mathrm{m})(1-\nu_\mathrm{m}/5)}{9(1-\nu_\mathrm{m}/2)}\rho\right]^{-1}, \tag{A17}$$

where ν_m is Poisson's ratio of the background material. Note that this theory can also be used for the seismic characterization of multiple fracture sets as described by Grechka and Tsvankin (2003). This can be done by using equation (2.19) of Kachanov (1992) for the calculation of K_N, K_V, K_H, K_NV, K_NH and K_VH in equation (5) of Grechka and Tsvankin (2003).

The Gassmann equation

The Gassmann equation (Gassmann 1951) predicts the elastic moduli of a fluid-saturated porous medium using the known elastic moduli of the solid matrix, the frame and the pore fluid. It is given by

$$\frac{K_\mathrm{sat}}{K_0 - K_\mathrm{sat}} = \frac{K_\mathrm{dry}}{K_0 - K_\mathrm{dry}} + \frac{K_\mathrm{fl}}{\phi(K_0 - K_\mathrm{fl})}, \tag{A18}$$

$$\mu_\mathrm{sat} = \mu_\mathrm{dry}, \tag{A19}$$

where K_dry denotes the effective bulk modulus of dry rock, K_sat denotes the effective bulk modulus of the rock with pore fluid, K_0 denotes the bulk modulus of the mineral making up the rock, K_fl denotes the effective bulk modulus of pore fluid, ϕ denotes the porosity, μ_dry denotes the effective shear modulus of dry rock and μ_sat denotes the effective shear modulus of rock with pore fluid. Again, in this equation both phases, the fluid and the mineral, are assumed to be continuous. This is not the case for isolated penny-shaped cracks. A more detailed discussion of the basic assumptions of the Gassmann equation can be found in Wang (2000).